Local structure in the stripe phase of $La_{1.6-x}Sr_xNd_{0.4}CuO_4$

S.-W. Han and E. A. Stern
Department of Physics, University of Washington, Seattle, Washington 98195-1560

D. Haskel
Advanced Photon Source, Argonne National Laboratory, Argonne, Illinois 60439

A. R. Moodenbaugh
Materials Science Department, Brookhaven National Laboratory, Upton, New York 11973-5000
(Received 25 January 2002; revised manuscript received 19 April 2002; published 4 September 2002)

We describe the *local* structure of crystalline $La_{1.6-x}Sr_xNd_{0.4}CuO_4$ ($x=0.12$, 0.16) in the temperature range 10–300 K as determined from orientation-dependent La *K*-edge x-ray absorption fine structure (XAFS) measurements. Such XAFS measurements of *c*-axis-aligned powders permit distinguishing like atoms at similar bonding distances because the measurement determines the angle of the bonds relative to the *c* axis. The *local* structure of $x=0.12$ about La atoms up to their fourth nearest neighbors, the distance which can reliably be probed by XAFS, does not correspond to any of the *average* periodic structures determined for this material by diffraction. The Cu-O_6 octahedra for $x=0.12$ are found to tilt $4.6°\pm0.4°$ from the *c* axis along an axis in the *a*-*b* plane $20.4°\pm5°$ from the *a* axis. This suggests the *Pccn* (LTO2) structure, though the octahedra become somewhat distorted and the more distant atoms do not fit the LTO2 structure. In contrast, the local structure of $x=0.16$ does fit the LTO2 structure and has corresponding tilt values of $3.8°\pm0.5°$ and $19.5°\pm7.5°$. The local structures for both concentrations are found to be independent of temperature, indicating that the various crystal phase transitions found in diffraction are due to long-range averaging of local structure regions with orientational disorder. The local structure correlation length appears to be longer than the high-T_c coherence length, indicating that the local structure is the relevant one when considering the pairing mechanism.

DOI: 10.1103/PhysRevB.66.094101 PACS number(s): 71.27.+a, 61.10.Ht

I. INTRODUCTION

It is generally recognized that knowledge of the structure of materials is fundamental to an understanding of their properties. The canonical method of determining this for crystalline materials is diffraction. However, it has been shown that for many cases the structure determined by diffraction does not correspond to the actual structure on the local interatomic scale.[1] The cause for this surprising fact is disorder on the local scale which is averaged out in the *average* periodic structure measured by diffraction. The local structure has a special importance for the high-T_c superconductors because of their short superconductivity coherence length of $\sim$10–20 Å. The pairing mechanism of superconductivity is determined by interactions between atoms in the volume of the dimensions of the coherence length. If the local structure has a correlation length larger than the superconductivity coherence length, then its structure is the relevant one for understanding the pairing mechanism, and not the average periodic structure as measured by diffraction. We have found local disorder in the Sr- and Ba-doped La_2CuO_4 high-T_c superconductors,[2,3] and the motivation of this investigation is to determine if local disorder is also present in $La_{1.6-x}Sr_xNd_{0.4}CuO_4$. This latter material is of great interest stirred by the discovery of static stripes by Tranquada, *et al.* in the low-temperature phase of the $x=0.12$ material by use of neutron diffraction.[4,5]

We employ the x-ray absorption fine structure (XAFS) technique to measure the local structure since it is best suited to investigate these materials[6] that are composed of a variety of atoms, some of which are minor component dopants randomly placed in the lattice. Of course site disorder is present in these materials due to the doping of Sr and Nd atoms; however, another type of disorder that can be detected by XAFS is displacements of atoms from the average periodic structure, which generally is expected around dopants. In particular, XAFS determines the partial pair distribution function about the probe atom whose absorption edge is excited. One can determine the local distortions around dopants by measuring XAFS above their absorption edges. However, in this paper we present the results of measurements of the XAFS from the *K* edge of La atoms, one of the host atoms, because we want to determine any disordering on the host lattice since the averaging of diffraction is most heavily weighted by them. The local structure determined by XAFS then can be directly compared to the diffraction structure, and any differences are due to disordering in the orientation of the local regions. The use of orientation-dependent XAFS on the sample composed of *c*-axis-aligned grains is essential for unambiguously determining the local structure of this complicated layered material. Making two independent XAFS measurements with the x-ray polarization parallel and perpendicular to the *c* axis not only doubles the information content of the data but also allows the separation of like atoms at similar bonding distances because the measurement also determines the angle of the bonds to the *c* axis.[2,3] If the sample consists of unoriented grains, then a spherical average is obtained and such a separation is not possible.

The crystal structures of the high-T_c superconductor $La_{1.6-x}Sr_xNd_{0.4}CuO_4$ have been widely investigated, particu-

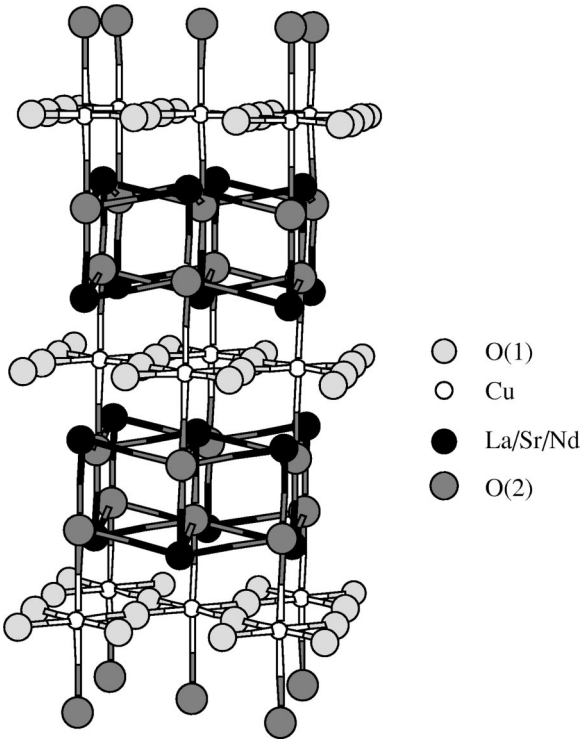

FIG. 1. The HTT phase of La_2CuO_4.

larly after the observation of the static stripe phase. Since the static charge ordering associated with the stripes distorts the low-temperature crystalline structure, its existence is detected by diffraction at superlattice diffraction peaks. X-ray and neutron diffraction measurements[4,5,7–10] found that the bulk structures of $La_{1.6-x}Sr_xNd_{0.4}CuO_4$ ($x=0.12\rightarrow0.16$) have a phase transition from a space group $Bmab$ (LTO1) $\rightarrow P4_2/ncm$ (LTT) at $\sim$60 K as the temperature is lowered from room temperature with a $Pccn$ (LTO2) phase intermediate between LTO1 and LTT for some range of x. The LTO1 phase is also designated as the LTO phase in earlier literature. Above room temperature these materials have another transition to the $I4/mmm$ (HTT) phase. The static stripe phase occurs in only the lowest-temperature LTT phase, though there may be dynamic stripes in the LTO1 phase.

All of the above phases have a simple relationship to one another consisting of Cu-O_6 octahedra tilts from the HTT high-symmetry phase. The difference between LTT, LTO1, and LTO2 can be visualized by starting with the HTT structure shown in Fig. 1. In this structure, the Cu-O_6 octahedra are oriented with their pair of oxygen apices along the (001) direction. In describing the rotations of the Cu-O_6 octahedra in HTT about axes in the a-b plane it is convenient to employ the common a and b axes of the LTO1, LTO2, and LTT structures, instead of those of HTT which are rotated by 45° about the c axis. The LTO1 structure has rotation axes along the a direction, passing through the Cu atoms, alternating from a right-handed to a left-handed rotation between neighboring unit cells along the b direction, leading to the elongation of the b axis relative to the a axis and the transition to the orthorhombic structure from the HTT tetragonal phase. The LTT phase is produced by alternating rotations about an

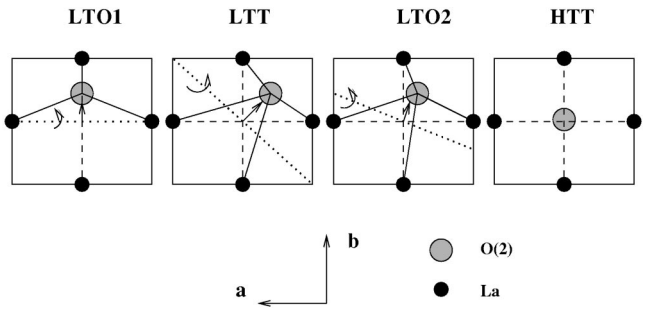

FIG. 2. Planar La-O distances for Cu-O_6 octahedra tilts for (left to right) LTO1, LTT, LTO2, and HTT. The oxygen atoms are the apical oxygens of the octahedra centered about Cu in the CuO_2 neighboring plane. Smaller correlated La displacements are neglected.

axis in the a-b plane, making a 45° angle with both a and b of the tetragonal HTT structure. In that case, the elongations along the a and b axes are the same, leading to the tetragonal LTT phase. The most general case of the alternating rotations is when the a- and b-axis components are not equal or zero, leading again to an orthorhombic phase, the LTO2 phase. In summary, the various low-temperature orthorhombic or tetragonal phases differ in the direction of their rotation axis in the a-b plane.

The rotation of the Cu-O_6 octahedra about the Cu atoms is almost rigid. The basal plane of the octahedron rotates rigidly but the apical oxygens rotate a slightly different angle so that the angle of the line connecting the apicals slightly deviates from being perpendicular to the octahedral basal plane. The rotation causes the apical O(2) oxygens (located in the neighboring La-O plane) to move in the La-O(2) planes from the center of their surrounding La as illustrated in Fig. 2 for the LTO1, LTT, and LTO2 structures, accompanied by the corresponding motion of the four planar octahedral O(1) oxygens, which causes a buckling of the Cu-O(1) planes. These O(1) and O(2) oxygens are nearest neighbors to the La atoms. It is important to note that the motion of these oxygens due to the rotation is the largest of all of the changes that occur between the three structures, and we use this feature to obtain the greatest sensitivity for discerning the local structure.

In fitting the local structure as determined by XAFS we are guided by our previous experience that the low-temperature local structure referred to the host atoms is the same as that determined by diffraction for *undoped* systems. However, for *doped* systems this is not a universal rule as we found for $La_{2-x}Sr_xCuO_4$, $x>0.20$,[2] and for the BKBO system[11] where the local structure was different in the lowest-temperature phase. We assume the local structure will satisfy the diffraction crystal structure at low temperatures as an initial guess and do the further analysis to refine the local structure.

In Sec. II, we discuss the experimental details of the preparation of $La_{1.6-x}Sr_xNd_{0.4}CuO_4$ ($x=0.12$, 0.16) samples and of the orientation-dependent La K-edge XAFS measurements from the samples. The analysis of the XAFS data and results are presented in Sec. III. We discuss the local struc-

ture of this material in Sec. IV and summarize the main conclusions in Sec. V.

II. EXPERIMENTAL DETAILS

Powder samples of crystalline $La_{1.6-x}Sr_xNd_{0.4}CuO_4$ ($x=0.12,\ 0.16$) were synthesized by the solid-state reaction technique. The details of the preparation of the samples are described elsewhere,[3,12] and the characterizations of the samples have been published.[12] Sintered pellets were ground and sieved to produce single-crystal grains about 1–3 μm, which is much smaller than the absorption length of ~ 122 μm, eliminating any significant distortion due to the thickness effect.[13] Then the grains were magnetically aligned with more than 95% of their c axes along the field as confirmed by x-ray diffraction (XRD).

For our XAFS measurements there are several advantages using powders of oriented single-crystal grains instead of single crystals: (a) Compositional homogeneity may be superior with ''powders.'' Often in crystals there are compositional variations, either along the growth axis (probably metal ratios) or from interior to surface (oxygen contents). There also may be non-214 inclusions in the ''crystal'' material. (b) It is possible to control the absorption thickness of powders so as to optimize the XAFS signal in transmission while typically single crystals are too thick for transmission, requiring fluorescence measurements with a consequent degradation of the signal from concentrated elements such as La. (c) Finally, we used the same powder material on which XRD measurements were made[12] so as to ensure that any differences seen between XRD and XAFS are not due to sample preparation.

Transmission measurements for the XAFS at the La K edge (38.925 keV) were performed at beamline X-11A of the National Synchrotron Light Source by using a Si (311) double-crystal monochromator. The energy resolution was $\Delta E \simeq 16$ eV at the La edge. For comparison, the core-hole lifetime broadening of the La K edge is ~ 20 eV.[14] The magnetically aligned samples were put in a gas tight copper cell with Kapton windows and indium seals, filled with He gas for thermal exchange, and attached to a cold finger of a displex refrigerator. Angular-dependent XAFS data were obtained by rotating the samples relative to the horizontal electric-field-polarized synchrotron radiation.

The samples were made and measured to have edge steps of $\Delta \mu x \sim 1$. Figure 3 shows total absorption (μx) at the La K-edge for the $x=0.12$ sample as a function of incident photon energy, measured at 10 K for orientations, $\hat{\varepsilon} \| \hat{c}$ and $\hat{\varepsilon} \perp \hat{c}$. The data are vertically shifted.

III. DATA ANALYSIS AND RESULTS

The x-ray absorption coefficient above the edge can be described by

$$\mu(k) = \mu_0(k)[1+\chi(k)], \tag{3.1}$$

where k is the photoelectron wave number relative to the Fermi wave number. For K edges ($1s$), the XAFS modulation can be written within the harmonic approximation for lattice vibrations[15] as

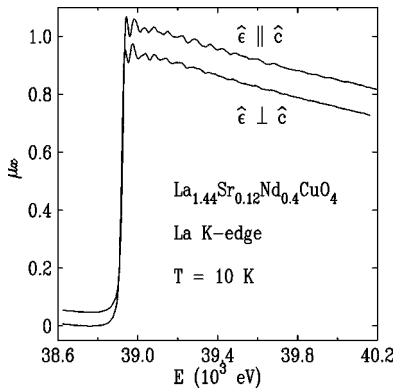

FIG. 3. Total x-ray absorption (μx) near the La K edge of $La_{1.48}Sr_{0.12}Nd_{0.4}CuO_4$ as a function of the incident x-ray energy at 10 K. The $\hat{c}$ axis was aligned parallel (top) and perpendicular (bottom) to the electric field vector of the x rays. The μx axis has an arbitrary origin and the two curves are shifted relative to one another.

$$\chi(k) = -\sum_j 3(\hat{\epsilon}\cdot\hat{r}_j)^2 \frac{S_0^2 N_j F_j(k,r_j)}{k r_j^2} e^{-2k^2\sigma_j^2} e^{-2r_j/\lambda(k)} \times \sin[2kr_j + \phi(k,r_j)], \tag{3.2}$$

where $\hat{\epsilon}$ is the electric field direction of the incident x rays, N_j is the coordination number of the jth shell of atoms, S_0^2 accounts for the change of the passive electron wave functions in the presence of a core hole, F_j is an effective curved wave backscattering amplitude, r_j is the effective interatomic distance, σ_j^2 is the mean-squared relative displacement in the effective interatomic distance, λ is an effective mean free path which includes the finite lifetime of the core hole, and ϕ is an overall scattering phase shift from the probe and jth backscattering atoms. Multiple-scattering paths are included in the analysis.

In order to analyze the measured XAFS data, we used the UWXAFS package.[16] First, $\chi(k)$ was extracted by subtraction of the atomic background $\mu_0(k)$ from the raw data $\mu(k)$. Figure 4 shows $k\chi(k)$. Comparing different scans, we conclude that the contribution of noise to the XAFS signal is significant for $k > 14.5$ Å^{-1}, especially for the $\hat{\varepsilon} \perp \hat{c}$ data. Since the absorption background varies substantially near the absorption edge, the uncertainty in χ is greatest there. To minimize these uncertainties only the XAFS data in the k range of 3.5–14 Å^{-1} were used for further analysis. Choosing the lower cutoff k point anywhere in the range 3–4 Å^{-1} produces insignificant variation of the fit parameters. $k^2\chi(k)$ was Fourier transformed to r space and fit to the theoretical XAFS calculations of FEFF7.[17] The dotted lines in Fig. 5 show the magnitudes of Fourier-transformed $k^2\chi(k)$. The abscissa $\tilde{r}$ is about 0.5 Å shorter than the true distances from the probing atom La because of the k dependence of $\phi(k,r_j)$. The range of the fit in $\tilde{r}$ is 1.7–5.5 Å as indicated by the vertical dashed lines. We call this the full range of the fit. Later we will fit only the first shell which covers the $\tilde{r}$ range of 1.7–2.7 Å.

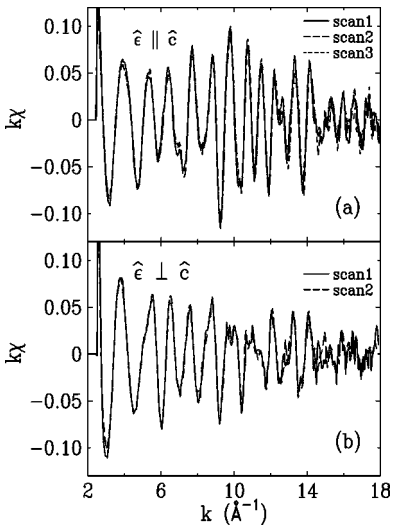

FIG. 4. XAFS, $k\chi(k)$, obtained from the previous figure as a function of photoelectron wave vector k. Three scans are shown for $\hat{\epsilon} \| \hat{c}$ and two scans for $\hat{\epsilon} \perp \hat{c}$.

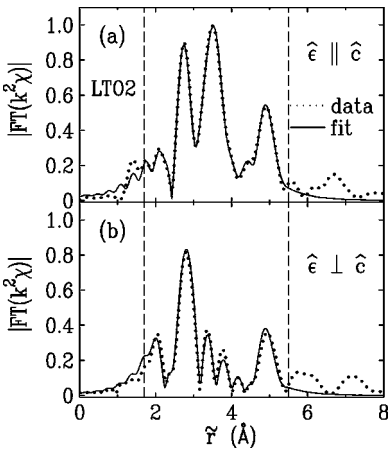

FIG. 5. Dotted curve is $\chi^{\text{expt}}(\tilde{r})$, the Fourier transform of the XAFS data $k^2\chi(k)$ of $La_{1.48}Sr_{0.12}Nd_{0.4}CuO_4$ at 10 K. Solid curve is a best fit assuming a modification from the LTO2 structure as described in the text. $\tilde{r}$ is the distance from the La probe atom without correction of phase shift. The two vertical dashed lines indicate the $\tilde{r}$ region over which the data were fit. The data were simultaneously fit for both orientations.

The theoretical fits to the data necessitate assuming a model with structural parameters which are varied so as to get an acceptable fit to the data. First we assume that at low temperatures there is no disorder so that the local structure is the same as the LTT given by the diffraction results.[4,5,7–10] If that does not give a satisfactory fit, then we repeat, assuming the other two diffraction determined structures for these materials: namely, LTO1 and LTO2. If a satisfactory fit is still not obtained, then we try to fit only the first shell of atoms with parameters consistent with the crystal symmetries of LTT, LTO1, and LTO2. The first shell of atoms are O(1) and O(2) atoms that, from crystal symmetry, comprise the oxygen portion of the Cu-O(1) octahedra. The different crystal symmetries allow the different directions of tilt of octahedra shown in Fig. 2. The symmetries require that the Cu-O(1) basal plane of the octaheda rotate rigidly. Finally, if none of the preceding gives satisfactory fits, then additional variables are added to allow a nonrigid rotation of the Cu-O(1) portion of the octahedra. As we find below, we need to proceed to the final step before obtaining a satisfactory fit.

A best full range $\tilde{r}=1.7$–5.5 Å fit was made for the LTT crystalline structure of $La_{1.6-x}Sr_xNd_{0.4}CuO_4$ ($x=0.12$) determined by powder neutron diffraction.[18] In the fit, only one σ^2 for each shell (defined as the same atoms at approximately the same distance) and E_0 for each type of atom independent of distance were variables. Single-scattering as well as multiscattering paths were included. Assuming that Nd and Sr dopants are randomly distributed on the La site, the theoretical χ's contributed by backscattering from La, Nd, and Sr atoms were obtained by adding them with weights: $(0.8\text{-}x/2)\times\chi_{La}+0.2\times\chi_{Nd}+(x/2)\times\chi_{Sr}$ for $La_{1.6-x}Sr_xNd_{0.4}CuO_4$ ($x=0.12$, 0.16). The two sets of XAFS data ($\hat{\epsilon} \| \hat{c}$ and $\hat{\epsilon} \perp \hat{c}$) were simultaneously fit to the XAFS theory.

The results of the best fit are given in Table I as the LTT[a] model. Goodness of fit criteria χ^2_ν, r factor, degrees of freedom ν, number of independent points in the data, $N_I=(2\Delta k\Delta\tilde{r})/\pi+2$, are defined in Refs. 3, 17, 19, and 20. Here $\Delta\tilde{r}$ and Δk are the range of $\tilde{r}$ and k space used for the analysis. The number of parameters P used in the fit is given by $P=N_I-\nu$. The parameters are listed further below for the LTO2 structure which has the largest number. A small value of the r factor $\lesssim 0.02$ (Ref. 16) indicates an acceptable fit was obtained. However, if $\chi^2_\nu \gg 1$, then this indicates that systematic errors dominate the uncertainty and rescaling $\epsilon \rightarrow \epsilon\sqrt{\chi^2_\nu}$ recovers the $\chi^2_\nu \approx 1$ criteria for a good fit. Uncertainties in the parameters, which are calculated by the change needed to increase χ^2_ν by $1/\nu$ from its minimum value (one standard deviation) and include the effect of correlations be-

TABLE I. Fits with different models at 10 K of the first shell consisting of O(1) and O(2) nearest neighbor atoms to the La probe atoms. LTT[a] is the local structure as determined by neutron diffraction measurements.

Model	χ^2_ν		r factor		σ^2 of planar oxygens (Å^2)		N_I	ν	
	$\Delta r=0$	$\Delta r\neq 0$	$\Delta r=0$	$\Delta r\neq 0$	$\Delta r=0$	$\Delta r\neq 0$		$\Delta r=0$	$\Delta r\neq 0$
LTT[a]	94.83		0.0870		0.0094(44)		17	12	
LTT	44.39	23.71	0.027	0.012	0.0115(56)	0.0163(62)	17	9	6
LTO1	50.84	42.66	0.021	0.016	0.0159(57)	0.0117(74)	17	9	6
LTO2	51.12	29.18	0.015	0.013	0.0035(6)	0.0031(4)	17	8	6

tween fitting parameters, are rescaled by $\sqrt{\chi^2_\nu}$. Two fits with similar values of ν are significantly different (two standard deviations) if the ratio $\chi^1_\nu/\chi^2_\nu \gtrsim (1+2\sqrt{2/\nu})$, the fit with the lowest χ^2_ν being better. The best fits presented here have r factor $\lesssim 0.02$ and $10 \lesssim \chi^2_\nu \lesssim 30$, indicating that systematic errors are ~ 3–6 times greater than statistical errors and are dominant.

Since an acceptable fit requires that the r factor be less than 0.02,[16] the r factor of LTT^a shows that its fit is not satisfactory. We conclude that the model of the crystal structure determined by Rietveld refinement of neutron diffraction data is not an accurate model for the *local* structure measured by XAFS. We denote this structure the LTT^a model in the discussion below.

We next investigate whether a satisfactory full range fit to the XAFS data can be obtained when we allowed not only σ^2 and E_0 to vary but also the LTT symmetry permitted x, y, and z values of the various atoms in place of varying each interatomic distance, separately. This assures that the crystal symmetry remains satisfied during the fit and has the added advantage of minimizing the number of variables. The fit was started with the atoms placed at the sites of the LTT structure determined by neutron diffraction.[18] ATOMS (part of the UWXAFS package) calculates atomic types and locations with given x, y, and z values, and FEFF7 (Ref. 17) is used to calculate theoretical XAFS for the atomic types and positions. The theoretical XAFS signal was fit to the measured XAFS data while varying x, y, z, σ^2, and E_0 using the FEFFIT program (part of the UWXAFS package) until a best fit is obtained. Since ATOMS calculates atomic positions with any given crystalline space group and its allowed x, y, and z values, the models for the crystalline structure can be controlled by choosing the desired crystalline space group in the input file of ATOMS. Again, a satisfactory fit was still not attained. We next repeated the last fitting procedure but now for the other crystalline phases found by diffraction below room temperature, the LTO1 and LTO2 phases. None of the full range fits were found to be satisfactory, though the LTO2 structure gave the closest fit.

Then the requirement of accurately maintaining the crystal symmetry was relaxed by allowing two additional parameters Δr's for each of the different types of oxygen nearest neighbors, i.e., the four La-O(2) planar oxygens and the one apical La-O(2) oxygen from the neighboring La-O plane and the four La-O(1) oxygens in the nearest Cu-O plane (see Fig. 6). The data did not support more uncorrelated parameters to determine the distortion in greater detail. Again the data were simultaneously fit for $\hat{\epsilon} \| \hat{c}$ and $\hat{\epsilon} \perp \hat{c}$. The required magnitudes of Δr were least for the assumed LTO2 structure, being less than 0.02 Å. The fits were better than without the Δr's but still not satisfactory. Figure 5 shows full range best fits (solid lines) for the initially assumed LTO2 structure for (a) $\hat{\epsilon} \| \hat{c}$ and (b) $\hat{\epsilon} \perp \hat{c}$. Figure 7 shows best fits (solid lines) for the initially assumed (a) LTT and (b) LTO1 structures for $\hat{\epsilon} \perp \hat{c}$. The $\hat{\epsilon} \perp \hat{c}$ data have the greatest sensitivity to detect the direction of the tilt angle (Fig. 2). The LTO2 $\hat{\epsilon} \perp \hat{c}$ fit is best for the first and second peaks (the first shell consists of oxygen

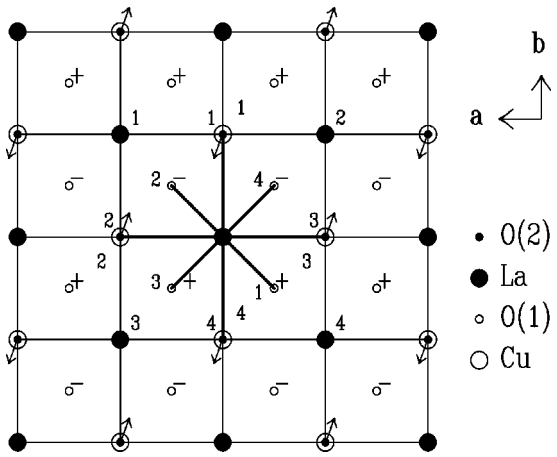

FIG. 6. A view from on top of the La-O(2) plane (solid circles) with the Cu-O(1) plane above (open circles) in the HTT phase of La_2CuO_4. The local tilt determined from XAFS is illustrated by the displacement of the O(1) and O(2) oxygens, as discussed in the text. Smaller correlated La displacements are neglected. The first neighbors to the center La atoms for $\hat{\epsilon} \perp \hat{c}$ are indicated by the thick solid lines. The numbers correspond to the atoms listed in Table II.

atoms most sensitive to Cu-O octahedral tilt while the second shell contains the Cu atoms of the octahedra in addition to the nearest planar La neighbors). However, at larger distances the modified LTO1 structure is preferable. Thus, none of the crystal symmetries give a satisfactory fit over the full range of the local structure determined by the XAFS data.

Since the first shell gives the most sensitivity for determining the direction of the tilts of the octahedra, we now limit our analysis to the first shell. We optimize the parameters used previously for fitting the three crystal symmetries over the full range, but now only for fitting the first shell range and with $\Delta r = 0$. The fit results for the nearest-neighbor oxygens of a La atom are summarized in Table I under the columns labeled $\Delta r = 0$. These best fits for nearest neighboring oxygens were obtained by refitting the data within $\tilde{r}$ of 1.7–2.7 Å by varying only the parameters which

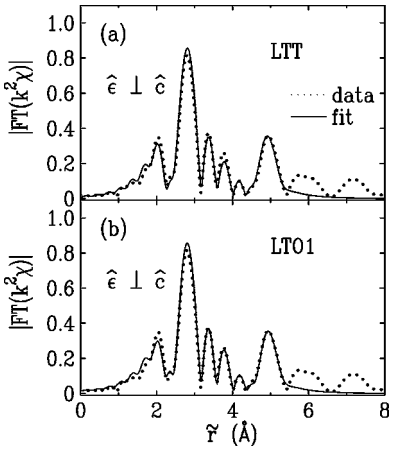

FIG. 7. Solid curve is a best fit with the 10 K data (dotted curve) for $x = 0.12$ and $\hat{\epsilon} \perp \hat{c}$, assuming modifications as described in the text of (a) the LTT and (b) the LTO1 structures.

TABLE II. The first two shells for the La probe local structure of $La_{1.48}Nd_{0.4}Sr_{0.12}CuO_4$ at 10 K. The first shell consists of the three types of oxygen atoms, and the second shell consists of four Cu atoms, and four La atoms. These atoms are labeled as shown in Fig. 6. The *x*, *y*, and *z* coordinates are the best fit assuming the LTO2 crystal structure and setting the origin at the La probe atom since XAFS measures the relative distances from the La probe to the neighboring atoms listed in the first column. The Δr's are the values that were required to add to the distances determined by the *x*, *y*, and *z* coordinates to obtain the best-fit distances from the La probe atom. Thus, the distance between the La probe atom and its neighbors is given by $(x^2+y^2+z^2)^{0.5}+\Delta r$. As discussed in Sec. IV the XAFS measurements did not have the resolution to distinguish the small differences in the La and Cu distances from an average distance and a mean-squared disorder σ^2 about the average. Only by assuming the LTO2 symmetry could these distances be individually distinguished. However, the XAFS measurements did have the resolution to distinguish the difference of the various crystal structures in their first-shell planar O(2) oxygens σ^2, and it was this capability that determined the local structure for this material to be LTO2.

Atom	x(Å)	y(Å)	z(Å)	Δr(Å)	r(Å)
La_1	2.637(10)	2.604(10)	0.0	0.0013(90)	3.707(13)
La_2	−2.684(10)	2.604(10)	0.0	0.0013(90)	3.741(13)
La_3	2.637(10)	−2.745(10)	0.0	0.0013(90)	3.809(13)
La_4	−2.684(10)	−2.745(10)	0.0	0.0013(90)	3.840(13)
Cu_1	−0.012(1)	2.639(10)	−1.827(7)	−0.0065(35)	3.203(10)
Cu_2	2.649(10)	−0.035(1)	−1.827(7)	−0.0065(35)	3.212(10)
Cu_3	−2.673(10)	−0.035(1)	−1.827(7)	−0.0065(35)	3.231(10)
Cu_4	−0.012(1)	−2.710(10)	−1.827(7)	−0.0065(35)	3.262(10)
$O(1)_1$	−1.342(5)	−1.373(5)	−1.687(7)	−0.0139(43)	2.542(11)
$O(1)_2$	1.318(5)	1.302(5)	−1.968(7)	−0.0139(43)	2.689(11)
$O(1)'_3$	1.318(5)	−1.373(5)	−1.763(7)	−0.0139(43)	2.580(11)
$O(1)'_4$	−1.342(5)	1.302(5)	−1.892(7)	−0.0139(43)	2.646(11)
$O(2)_1$	0.054(1)	2.461(9)	0.538(2)	−0.0117(40)	2.508(11)
$O(2)_2$	2.583(10)	0.1430(5)	0.538(2)	−0.0117(40)	2.631(11)
$O(2)_3$	−2.738(10)	0.1430(5)	0.538(2)	−0.0117(40)	2.782(11)
$O(2)_4$	0.054(1)	−2.888(10)	0.538(2)	−0.0117(40)	2.926(11)

contribute to the first oxygen shells, including the *x*, *y*, and *z* values, while keeping the parameters in the $\tilde{r}$ region from 2.7 to 5.5 Å fixed at their values determined by the fit of the data within the full $\tilde{r}$ range of 1.7–5.5 Å. This effectively subtracts the contribution from the atoms beyond the first-neighbors that overlaps the first neighbor fitting range. None of the models fit well in the $\Delta r=0$ columns. The LTO2 model satisfies only the *r* factor criterion, while the others satisfy none. Thus, we find that a rigid tilt of the Cu-O(1) octahedral basal planes cannot fit the local structure as determined by the XAFS measurements. The LTT, LTO1, and LTO2 models exhaust all of the possible rigid basal plane tilt rotations about axes in the *a*-*b* plane.

We next relax the condition of a rigid tilt of the Cu-O(1) octahedral basal planes by adding, as done previously over the full range, the variables Δr_1 and Δr_2 to the La-O(1) and La-O(2) distances, respectively, determined by the *x*, *y*, and *z* variables. The best fits are presented in Table I under the column $\Delta r\neq 0$. Here there is a significant improvement in both χ_ν^2 and the *r* factor for all three structures: LTT, LTO1, and LTO2. All three structures now satisfy the *r*-factor criterion, and the LTO1 has a χ_ν^2 value only a standard deviation worse. However, note that the σ^2 of the O(2) atoms is much larger for the LTT and LTO1 than for the LTO2 structure. The σ^2 is a measure of both the vibrational and structural disorder. The vibrational motion at 10 K is zero-point motion which can be determined by requiring consistency with the temperature dependence that we discuss below and show in Fig. 9, below. The LTO2 structure has the σ^2 value of the zero-point motion while the LTT and LTO1 structures require an additional structural disorder to explain its value.

The question then arises whether the 0.013 $Å^2$ (or 0.009 $Å^2$) increase in structural disorder of the O(2) is due to choice of the wrong model or reflects disorder caused by the random occurrence of Sr and Nd on the La site inherent in the structure. Assuming that the disorder occurs primarily at nearest neighbor sites of Nd atoms[2] and taking into account that only 20% of the sites have Nd nearest-neighbors, the σ^2 structural disorder at O(2) is an order of magnitude greater than that induced by the difference between Nd and La radii of 0.07 Å. Thus we conclude that the large structural disorder for LTT and LTO1 structures is due to the choice of an inappropriate model, and only the modified LTO2 model fits the XAFS data for the first-shell La neighbors.

Table II presents the *x*, *y*, and *z*, and Δr values from the La-probe atom of its first three shells. The first shell consists of the O(1) and O(2) oxygens while the overlapping second and third shells (producing the second peak at about $\tilde{r}=2.7$ Å in Fig. 5) consist of the Cu and La atoms, respectively. The *x*, *y*, and *z* values satisfy the symmetry of the

LTO2 structure while the Δr values weakly break this symmetry to obtain a best fit to the local structure. Theory predicts that S_0^2 is independent of temperature. This was verified by fitting the data measured at 13 temperatures from 10 to 300 K, giving an average value of $S_0^2 = 0.97 \pm 0.01$. In the subsequent fits S_0^2 was fixed at 0.97.

The LTO2 fits to the first-neighbor oxygens over the $\tilde{r}$ range 1.7–2.7 Å given in Table I used 9 parameters for $\Delta r = 0$ and 11 for $\Delta r \neq 0$ with the origin at the probe La atom. These parameters for $\Delta r = 0$ are E_0, an energy shift of ~ 1 eV to correct the scattering phase shift from the nearest-neighbor oxygen atoms; three σ^2, one each for the O(1) atoms, the planar O(2) atoms, and the apical O(2) atom; the *x*, *y*, and *z* for the O(2) atoms; and one *z* each for the O(1) and O(1)′ atoms. Two more parameters were added for $\Delta r \neq 0$: namely, one Δr each for the O(1) and O(2) atoms. In Table II the fit range of $\tilde{r}$ was 1.7–5.5 Å, increasing N_I by 37, while the addition of the Cu and La atoms required 19 more parameters for the best fit, namely, 6 *x*, *y*, and *z* for the La and Cu atoms; 2 E_0's for the La and Cu atoms; 8 σ^2 for the various scattering paths; and 3 significant Δr's. Thus, including the nearest-neighbor oxygen shell of Table I, there are 54 independent data points N_I and 30 parameters *P*, giving 24 degrees of freedom ν in the fit that determines the values listed in Table II. The quantities shown in Table II are only the ones in the first two shells of Fig. 5 containing the nearest oxygen, Cu, and La atoms.

From the *x*, *y*, and *z* values in Table II of the best fit of the modified LTO2 structure, the rotation of the copper-oxygen octahedron[7] can be determined by calculating the positions of the oxygens in the La plane relative to the position of the center Cu atom,[3] as noted above and illustrated in Fig. 2. The tilt angle of the octahedron relative to the *c* axis is found to be $4.6° \pm 0.4°$ and the rotational axis of the octahedron is $20.4° \pm 5°$ from the *a* axis. The rotational axis found by the XAFS is that of the LTO2 structure and is about half way between the LTO1 and LTT structures. The *x*, *y*, and *z* values employed satisfy the LTO2 crystal symmetry and represent a rigid tilt of the octahedra. The Δr corrections are only of the order of 0.02 Å, and the introduced nonrigidity causes an insignificant uncertainty in the tilt.

As discussed in Sec. III the small value of the *r* factor indicates that a good fit has been achieved but the large χ_ν^2 indicates that systematic errors introduced by background subtraction uncertainties, theory approximations, and measurements are dominant. The quoted uncertainties of the parameters in the tables and the text include the contribution of the systematic errors.

We analyzed the 300 K data with the same procedure as the 10 K data, except that we also considered the HTT structure. Figure 8 shows the magnitude of the Fourier-transformed XAFS data (dotted line) at 300 K for $\hat{\epsilon} \perp \hat{c}$ with best fits (solid lines), simultaneous for both polarizations, for the four structures. The distinctions between the various models can be determined in the low-$\tilde{r}$ region, < 4.5 Å, where signal-to-noise ratio is favorable. Best fits are summarized in Table III. We conclude that the room-temperature

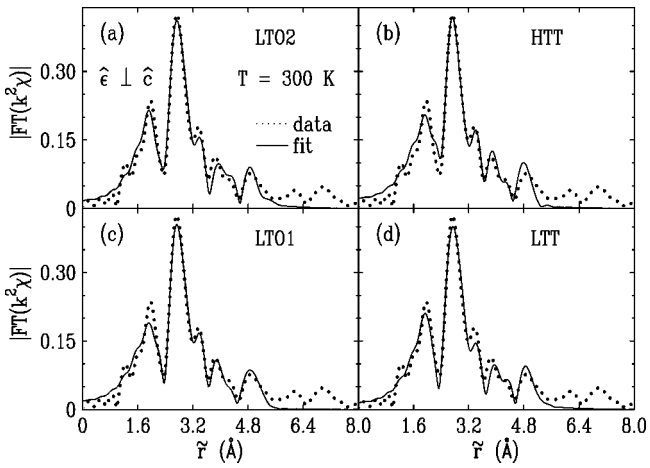

FIG. 8. Magnitude of Fourier-transformed La *K*-edge $k^2\chi(k)$ data of the $x = 0.12$ sample (dotted curves) for $\hat{\epsilon} \perp \hat{c}$ at 300 K, and best fits (solid curves) with different models, assuming modifications as described in the text, of the (a) LTO2, (b) HTT, (c) LTO1, and (d) LTT structures.

structure of the first neighbor O(2) atoms (LTO2 modified by Δr) is similar to the 10 K structure, within uncertainties.

We analyzed XAFS data of $La_{1.48}Sr_{0.12}Nd_{0.4}CuO_4$ in the temperature range 10–300 K with the same procedure used for the endpoints. Figure 9 shows parameters as a function of temperature. There being four separate distances [Fig. 9(a)] observed for planar oxygen throughout is consistent with LTO2; no structural transition is indicated. In Fig. 9(b) the temperature dependent σ^2 fits an Einstein model[21] with $\Theta_E = 450 \pm 16$ K. The reduced mass m_r used in calculating Θ_E was the usual $m_r^{-1} = m_O^{-1} + m_{La}^{-1}$, where m_O is the mass of an oxygen atom and m_{La} is the mass of a La atom. This is consistent with an absence of disorder introduced by a structural phase transition (any such mean-square disorder must be < 0.0015 Å^2, the measurement uncertainty).

For near optimally doped $La_{1.44}Sr_{0.16}Nd_{0.4}CuO_4$, orientation-dependent XAFS measurements at the La *K* edge were also performed for the temperature range of 10–300 K. At 10 K, a best fit to the XAFS data finds that the local structure fits the LTO2 crystalline structure throughout the whole $\tilde{r}$ range, in contrast to the $x = 0.12$ sample; i.e., the structure is consistent with a rigid tilt. The tilt angle of the Cu-O octahedron to the *c* axis is found to be $3.8° \pm 0.5°$ and the rotational axis of the octahedron is $19.5° \pm 7.5°$ from the *a* axis. The tilt angle is marginally smaller than, while the

TABLE III. Fits with different models at 300 K of the first shell consisting of O(1) and O(2) nearest-neighbor atoms to the La probe atoms.

Model	χ_ν^2	*r* factor	σ^2 of planar oxygens (Å^2)	N_I	ν
LTO2	11.90	0.015	0.0076(11)	16	5
HTT	13.06	0.019	0.0278(45)	16	7
LTO1	16.80	0.020	0.0124(49)	16	5
LTT	10.26	0.012	0.0127(24)	16	5

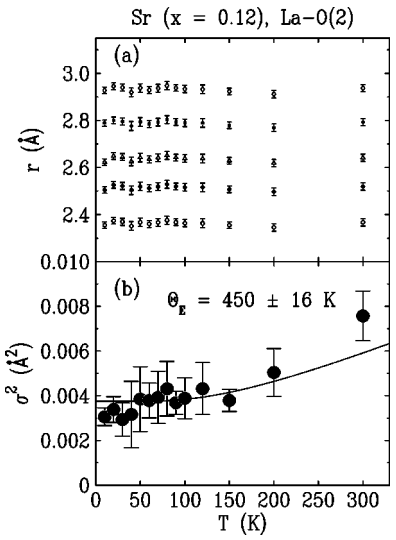

FIG. 9. (a) The distances and (b) σ^2 of the nearest O(2) oxygens from the La probe atom in the La-O(2) plane as a function of temperature for $x=0.12$. The top four plots in (a) are for the planar O(2) oxygens and the bottom is for the apical O(2) oxygen along the c direction. The solid line in (b) is a best fit with an Einstein model and and $\Theta_E=450\pm16$ K.

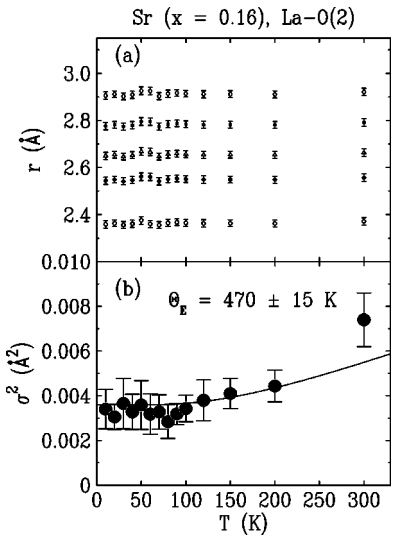

FIG. 10. The same results as in the previous figure but for the $x=0.16$ sample.

rotational axis angle is consistent with, those of the $x=0.12$ material, though the uncertainties are somewhat larger because the data had more noise. Figure 10 shows the same information as Fig. 9 does for the $x=0.12$ sample. Again, no structural transition was detected and the local structure remained LTO2 over the temperature range 10–300 K. A best fit, solid line in (b), of an Einstein temperature of $\Theta_E=470\pm15$ K gives a similar σ^2 temperature dependence as found in the $x=0.12$ doped material.

IV. DISCUSSION

As pointed out in the Introduction, diffraction by x rays[7–9] and neutrons[10,18] found the crystalline structure of $La_{1.48}Sr_{0.12}Nd_{0.4}CuO_4$ at low temperature to be LTT. XAFS measurements, which determine the local structure, have the capability to determine with high resolution the relative distances between the probe atom, La in this case, and its surrounding atoms. Resolution is the ability to distinguish between separate distances and a mean-squared disorder σ^2 about the average distance. It is given by $\delta r_{min}=\pi/(2k_{max})=0.11$ Å, where $k_{max}=14$ Å^{-1} in our measurements. This criterion is the condition that a beat occur in $\chi(k)$ due to the separation δr_{min} (Ref. 6), and is analogous to the Rayleigh criterion for resolving two points with light. When more than two distances are close together as is the case here, then the resolution estimate for two distances is a lower limit. The resolution realized by $k_{max}=14$ Å^{-1} is the same as that by scattering of x rays or neutrons of wave number transfer $q=2k_{max}=28$ Å^{-1}. As can be noted in Table II the oxygen atoms are the ones that can be most clearly resolved by XAFS and it was this capability that helped the XAFS to choose the LTO2 local structure from the other structures. The fact that the modified LTO2 structure also gave a good fit to the second peak in Fig. 5 consisting of the second shell Cu and third shell La atoms, and the modification needed for this best fit was less than $\Delta r=0.01$ Å, justify using the crystal symmetry to distinguish the various La and Cu distances as listed in Table II.

Our XAFS study found that the local structure is independent of temperature and does not fit any of the crystal structures found by diffraction; namely, LTT, LTO1, LTO2, or HTT. In all the tilted *crystalline* phases (LTT, LTO1, LTO2) the octahedra rigidly rotate their basal planes consisting of the interior Cu atom surrounded by its four nearest-neighbor O(1) atoms. As shown in Fig. 6, the octahedra share each of their O(1) base atoms with a single neighboring octahedron, and this coupling produces a periodicity in the Cu-O(1) plane of neighboring octahedra rotating in alternating sense to each other. The periodicity requires the rigid rotation of the Cu-O(1) base. The axis of rotation of each octahedron passes through the Cu atoms so that for small rotations the O(1) atoms move perpendicular to the plane of Fig. 6 and are denoted by $+(-)$ signs for motion up (down) along the c axis.

We find for the $x=0.12$ sample that *locally* the tilt angle is $4.6°\pm0.4°$; the rotation axis in the a-b plane of the local structure makes an angle about halfway between the LTT and LTO1 phases and, thus, is closest to the LTO2 phase. However, the rigidity of the octahedral basal planes is lost, so the LTO2 periodicity is not imposed. An local density approximation (LDA) calculation[22] of the band structure of La_2CuO_4 found that the HTT phase with no tilt is unstable at an energy maximum, consistent with the XAFS result of the octahedra remaining tilted locally at all temperatures. The $x=0.16$ sample had a marginally smaller tilt angle of $3.8°\pm0.5°$, and within uncertainty had the periodicity of the LTO2 structure. Thus, there was some change in the local structure between $x=0.12$ and 0.16.

The apparent discrepancy between the XAFS and diffrac-

tion results is related to the fact that diffraction and XAFS measure different structures. Whereas XAFS measures the local structure, i.e., the partial pair distribution function,[1,6] diffraction measures the average periodic structure. These two are not equivalent when local disorder is present. For the case at hand, the local structure can be disordered in such a manner that the *a* and *b* axes randomly interchange with one another, so that the local orthorhombic regions average to a tetragonal LTT structure. Similarly, the LTO1 structure is obtained from the local structure by a disordering such that the O(2) atom in Fig. 2 equally occupies the sites related by inversion symmetry about the *b* axis of the LTO2 structure. After this averaging only the component of the tilt angle along the diagonal for LTT remains, while only the tilt angle along the *b* axis remains for LTO1. In both cases the same magnitude of tilt remains, namely, $4.6\times(\cos 22.5°)=4.2° \pm 0.4°$, in good agreement with the value of 4.4° found by diffraction measurements.[18] Each local region must have dimensions in the nanometer range, too small to produce diffraction peaks, so that diffraction measures only the average LTT or LTO1 structure, respectively.

Such disordering of the tilt angle producing LTT can be accomplished, for example, by the Cu-O_6 octahedra tunneling so that the O(2) oxygen atoms move to the equal energy site obtained by reflection about the diagonal of the LTO2 square in Fig. 2. Similarly, octahedra tunneling or hopping can occur so that the LTO1 average phase is produced. Finally, the HTT phase can be obtained at high temperatures where the hopping can overcome all barriers so that all of the eightfold equivalent O(2) sites of equal energy[22] of the LTO2 square in Fig. 2 (found by reflection about the fourfold equivalent axes) are equally occupied.

The LTO2 structure apparently found by diffraction between the LTT and LTO1 phases for a limited range of *x* values as a function of temperature is peculiar. This is in violation of the usual behavior of the higher-temperature state being more symmetric. In our model more symmetry has more orientational disordering of the local order regions and thus more entropy as expected for higher temperature phases. As far as we could ascertain, the structure of the intermediate LTO2 phase has not been refined. It would be worthwhile to do more detailed measurements in this region of phase diagram space to determine the tilt angle of the intermediate LTO2 phase. Because of the averaging, the tilt angle decreases from the local value by about 0.4° in the LTT and LTO1 structures. If the LTO2 phase is the same as our local structure, then our results would predict that its tilt would be 0.4° greater than in the LTT and LTO1 phases. However, accurate refinement is difficult since phase mixtures are common and peak widths of LTO2 $(h00)/(0k0)$ peaks are broadened relative to the rest of the pattern.

The XAFS results are experimental evidence that the structural phase transformations occurring in $La_{1.6-x}Sr_xNd_{0.4}CuO_4$ ($x=0.12$, 0.16) have a significant amount of order-disorder character and are not due simply to an instability of a soft mode as has been previously suggested.[18] Similar significant order-disorder nature of structural phase transitions was also found from XAFS measurements on the local structures of the high-T_c superconductors $La_{2-x}Sr_xCuO_4$ (Ref. 2) and $La_{2-x}Ba_xCuO_4$ (Ref. 3). In addition, significant order-disorder nature of structural ferroelectric and antiferrodistortive rotational phase transitions has been seen in other perovskitelike materials.[1,11]

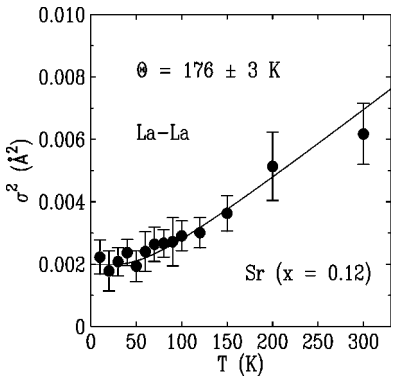

FIG. 11. The σ^2 of the La-La distances which define the *a* and *b* lattice constants in the crystalline structure, shown as a function of temperature. The solid line is a best fit with $\Theta_E=\sim 176$ K, using a standard reduced mass equal to half of the La atom mass.

Büchner *et al.*[23] showed from x-ray diffraction that the maximum tilt angle of the octahedron for bulk superconductivity is $\sim 3.6°$. The T_c of our $x=0.16$ sample is 14 K and the $x=0.12$ sample does not have a bulk transition to 2 K.[12] The tilt angles of the octahedra are $4.6\pm 0.4°$ and $3.8 \pm 0.5°$ for the $x=0.12$ and 0.16 doped materials, respectively, qualitatively agreeing with Büchner *et al.*

We next discuss whether our measurements detected any signature of the periodic distortions of static stripes for the $x=0.12$ sample that produce the superlattice peaks. To do this we have determined as a function of temperature the σ^2 of La-La distances for the nearest-neighbor La atoms to the center La in the La-O(2) plane shown in Fig. 6. These results are plotted in Fig. 11. When there are a variety of such distances as in these Nd doped materials the σ^2 determined by XAFS is a more sensitive measure of a change in distances than the directly determined La-La distances. The data are fit well by a single $\Theta_E \simeq 176$ K, and we do not see any discontinuity from a transition within uncertainties. With the fluctuations about the theoretical plot of 0.0002 Å^2 the rms change in these La-La distances is less than 0.014 Å at the LTT-LTO1 phase transition temperature of ~ 60 K, which is also the upper temperature region of static stripes in $La_{1.6-x}Sr_xNd_{0.4}CuO_4$ ($x=0.12$). The stripes may be present as dynamic ones in the LTO1 phase, explaining our lack of detecting any discontinuity, but we suggest that XAFS does not have the sensitivity to detect the distortions produced by stripes. Tranquada *et al.*[5] estimated that the oxygen displacement of Cu-O is about 0.004 Å which is smaller than the 0.014 Å uncertainty of our XAFS measurements and thus undetectable. Since the charged stripes are concentrated in the Cu-O(1) planes, the induced distortions are expected to be largest there and thus even smaller in the La-O(2) plane where our measurement focused, so that there is no surprise that we did not detect a signal from stripes. Using measurements with Cu as the probe atom one can focus in the Cu-

O(1) plane where the distortions due to stripes are largest. But even there the XAFS uncertainties are too large to detect them if they are as small as estimated.[5] There have been some previous claims that Cu *K*-edge XAFS detected the presence of stripes that produced lattice distortions of 0.04 Å in other La_2CuO_4 based materials,[24] but subsequent more sensitive XAFS measurements about the Cu atoms[3,25] do not support these early measurements, and it is now quite certain that the structural distortions induced by the stripes are well below the detection limit of XAFS in these materials, even about the Cu atoms.

In the above discussion we have assumed that though locally the tilt angle of the Cu-O_6 octahedra from the *c* axis is constant in magnitude and makes a fixed angle to the *a* axis, it does not follow that all of the octahedra are oriented the same. In fact the disordering of the orientation of the local regions is necessary to explain the difference in structure found by diffraction and XAFS. To understand this issue better, it is necessary to realize that XAFS cannot determine the absolute direction of the *a* axis for our sample which was randomly oriented about the *c* axis. Remembering that if the Cu-O(1) basal plane of the octahedron tilts rigidly, long-range orientational order occurs, and it follows from continuity that the greater the deviation from this rigidity, the shorter the orientational correlation length would be. Since the deviation from rigidity is small for the $x=0.12$ sample as shown in Table II by the small values of Δr relative to the rotational displacements, it is reasonable to expect that the orientational correlation length would be significantly more than a single unit-cell dimension in the *a*-*b* plane (5.34 Å) but with an upper limit less than about 100 Å so as not to be seen in diffraction. Because the coherence length of superconductivity in the Cu-O(1) plane is about 20 Å, one expects that it would be of the order or less than the orientational correlation length. This is even more true for the $x=0.16$ sample which showed even less deviation from periodicity.

Since the superconductivity pairing mechanism is determined in the volume of the dimensions of the coherence length, the local structure and not the average periodic structure as measured by diffraction is relevant for understanding the mechanism. We have shown that the local structure is independent of temperature, which predicts that T_c should not be affected by the structural phase transitions found by diffraction. In the materials investigated here the structural phase transitions occur at temperatures well above T_c and thus one cannot detect the lack of dependence on the structural phase transitions. However, $La_{2-x}Sr_xCuO_4$ does show this behavior[2] near $x=0.21$ where a boundary between LTO1 and HTT passes below T_c, yet there is no evidence of any effect on the *x* dependence of T_c. On the other hand, long-range structure is relevant to properties that may depend on dimensions larger than the local structure correlation length such as carrier transport and stripes (mean free path for the former and size of stripes for the latter).

Recent measurements by angle-resolved photoemission spectroscopy[26] and inelastic neutron scattering[27] have presented evidence that there is strong coupling between the carriers in $La_{2-x}Sr_xCuO_4$ and optical vibration modes involving the Cu-O(1) basal atoms of the octahedra. Since we show that the orientation of the octahedra is disordered, either dynamically or spatially, any theory which accounts for the strong carrier and lattice coupling should investigate the importance of this disordering effect.

V. CONCLUSIONS

The local structure of $La_{1.6-x}Nd_{0.4}Sr_xCuO_4$ ($x=0.12$, 0.16) for the temperature range of 10–300 K was determined by orientation-dependent XAFS at the La *K* edge. It was found to consist of tilts of the Cu-O_6 octahedra, similar to the LTO2 structure, with a tilt angle to the *c* axis of $4.6°\pm0.4°$ for $x=0.12$ and $3.8°\pm0.5°$ for $x=0.16$, oriented about halfway between the LTO1 and LTT structures, independent of temperature. The rotations of the octahedra are not quite periodic for $x=0.12$ while they are more periodic for $x=0.16$. The temperature independence of the local structure is in contrast to the several different phase transitions in the average periodic structure as determined by diffraction over the same temperature range. The difference between average and local structures occurs because of orientational disordering between various regions of LTO2 local order with a short *correlation* length. This significant order-disorder character to the structural phase transitions is evidence that the structural phase transitions are not caused simply by soft phonon mode instabilities as previously suggested. One result of the disordering is that the averaged tilt angle of the diffraction determined LTO1 and LTT phases is about 0.4° smaller than the local structure tilt. If the structure of the LTO2 diffraction phase at an intermediate temperature between the LTT and LTO1 phases can be refined, our model would predict that its local tilt would be 0.4° larger, assuming it is the structure with *Pccn* symmetry.

One is tempted to suggest that the change in local structure between $x=0.12$ and 0.16 is caused by the existence of static stripes in the $x=0.12$ sample. However, the change in Sr doping causes other effects that may affect the local structure. The higher doping increases the carrier concentration and changes the mix of Sr and La ions in the sample. This induces a change in the interaction between the carriers and lattice, and it would take a detailed theoretical investigation well beyond the scope of this study to understand the cause of the change.

Because of the even shorter *coherence* length of the high-T_c superconductor $La_{1.6-x}Nd_{0.4}Sr_xCuO_4$ than the *correlation* length, the local structure is the one relevant to the pairing mechanism and not the diffraction structure.

It is suggested that any consideration of the strong carrier-lattice interaction involving the energetic optical breathing mode in the Cu-O(1) plane of the octahedra include the effect of the disordering of the tilting orientation of the Cu-O_6 octahedra.

ACKNOWLEDGMENTS

One of the authors (E.A.S.) is pleased to acknowledge very informative discussions with Professor Yizhak Yacoby and Dr. John Tranquada. Work at the University of Washing-

ton was done under auspices of DOE Grant No. DE-FG03-98ER45681, work at Brookhaven National Laboratory was supported by the Division of Materials Sciences and the Division of Chemical Sciences, Office of Basic Energy Sciences, Office of Science, DOE Contract No. DE-AC02-98CH10886, and work at Argonne was supported by the U.S. DOE, Office of Science, under Contract No. W-31-109-ENG-38.

[1] Y. Yacoby and E.A. Stern, Comments Condens. Matter Phys. **18**, 1 (1996).

[2] D. Haskel, E.A. Stern, D.G. Hinks, A.W. Mitchell, J.D. Jorgensen, and J.I. Budnick, Phys. Rev. Lett. **76**, 439 (1996); D. Haskel, E.A. Stern, D.G. Hinks, A.W. Mitchell, and J.D. Jorgensen, Phys. Rev. B **56**, 521 (1997).

[3] D. Haskel, E.A. Stern, F. Dogan, and A.R. Moodenbaugh, Phys. Rev. B **61**, 7055 (2000).

[4] J.M. Tranquada, B.J. Sternlieb, J.D. Axe, Y. Nakamura, and S. Uchida, Nature (London) **375**, 561 (1995).

[5] J.M. Tranquada, J.D. Axe, N. Ichikawa, Y. Nakamura, S. Uchida, and B. Nachumi, Phys. Rev. B **54**, 7489 (1996).

[6] E.A. Stern, in *Phase Transitions and Self Organization in Electronic and Molecular Networks*, edited by M.F. Thorpe and J.C. Phillips (Kluwer Acad./Plenum, New York, 2001), pp. 209–224.

[7] M.K. Crawford, R.L. Harlow, E.M. McCarron, W.E. Farneth, J.D. Axe, H. Chou, and Q. Huang, Phys. Rev. B **44**, 7749 (1991); M.K. Crawford *et al.*, in *Lattice Effects in High-T_c Superconductors*, edited by Y. Bar-Yam, T. Egami, J. Mustre-DeLeon, and A.R. Bishop (World Scientific, Santa Fe, New Mexico, 1992), pp. 531–541.

[8] A.R. Moodenbaugh, Lijun Wu, Yimei Zhu, L.H. Lewis, and D.E. Cox, Phys. Rev. B **58**, 9549 (1998).

[9] B. Büchner, M. Cramm, M. Braden, W. Braunisch, O. Hoffels, W. Schnelle, R. Müller, A. Freimuth, W. Schlabitz, G. Heger, D.I. Khomskii, and D. Wohlleben, Europhys. Lett. **21**, 953 (1993); B. Büchner, M. Braden, M. Cramm, W. Schlabitz, W. Schnelle, O. Hoffels, W. Braunisch, R. Müller, G. Heger, and D. Wohlleben, Physica C **185-189**, 903 (1991).

[10] J.M. Tranquada, N. Ichikawa, and S. Uchida, Phys. Rev. B **59**, 14 712 (1999).

[11] Y. Yacoby, S.M. Heald, and E.A. Stern, Solid State Commun. **101**, 801 (1997).

[12] A.R. Moondenbaugh, L.H. Lewis, and S. Soman, Physica C **290**, 98 (1997).

[13] K.-Q. Lu and E.A. Stern, Nucl. Instrum. Methods Phys. Res. **212**, 475 (1983).

[14] O. Keski-Rahkonen and M.O. Krause, At. Data Nucl. Data Tables **14**, 139 (1974).

[15] E.A. Stern, Phys. Rev. B **10B**, 3027 (1974); J.J. Rehr and R.C. Albers, Phys. Rev. B **41**, 8139 (1990); J.J. Rehr, R.C. Albers, and S.I. Zabinsky, Phys. Rev. Lett. **69**, 3397 (1992).

[16] E.A. Stern, M. Newville, B. Ravel, Y. Yacoby, and D. Haskel, Physica B **208&209**, 117 (1995). Find further information of UWXAFS at http://depts.washington.edu/uwxafs

[17] A.L. Ankudinov and J.J. Rehr, Phys. Rev. B **56**, R1712 (1997).

[18] J.D. Axe and M.K. Crawford, J. Low Temp. Phys. **95**, 271 (1994).

[19] E.A. Stern, Phys. Rev. B **48**, 9825 (1993).

[20] M. Newville, B. Ravel, D. Haskel, J.J. Rehr, E.A. Stern, and Y. Yacoby, Physica B **208&209**, 154 (1995).

[21] E. Sevillano, H. Meuth, and J.J. Rehr, Phys. Rev. B **20**, 4908 (1979).

[22] W.E. Pickett, R.E. Cohen, and H. Krakauer, Phys. Rev. Lett. **67**, 228 (1991).

[23] B. Büchner, M. Breuer, A. Freimuth, and A.P. Kampf, Phys. Rev. Lett. **73**, 1841 (1994).

[24] A. Lanzara, N.I. Saini, T. Rossetti, A. Bianconi, H. Oyanagi, H. Yamaguchi, and Y. Maeno, Solid State Commun. **97**, 93 (1996).

[25] T. Niemöller, B. Büchner, M. Cramm, C. Huhnt, L. Tröger, and M. Tischer, Physica C **299**, 191 (1998).

[26] A. Lanzara, P.V. Bogdanov, X.J. Zhou, S.A. Kellar, D.L. Feng, E.D. Lu, T. Yoshida, H. Eisaki, A. Fujimori, K. Kishio, J.-I. Shimoyama, T. Noda, S. Uchida, Z. Hussain, and Z.-X. Shen, Nature (London) **412**, 510 (2001).

[27] R.J. McQueeney, J.L. Sarrao, P.G. Pagliuso, P.W. Stephens, and R. Osborn, Phys. Rev. Lett. **87**, 077001 (2001).